



## CALCULATION OF THE MECHANICAL PROPERTIES OF FeB LAYER'S BY FINITE ELEMENT METHOD

Osman Culha<sup>1</sup>, Mustafa Toparli<sup>1</sup>, Tevfik Aksoy<sup>1</sup> and Mustafa Akdag<sup>2</sup>

<sup>1</sup>Dokuz Eylul University, Engineering Faculty, Department of Metallurgical and Materials Engineering, Buca, 35160, Izmir, Turkey  
osman.culha@deu.edu.tr, mustafa.toparli@deu.edu.tr, tevfik.aksoy@deu.edu.tr

<sup>2</sup>Gediz University, Engineering and Architecture Faculty, Department of Mechanical Engineering, Cankaya, 35210, Izmir, Turkey  
mustafa.akdag@gediz.edu.tr

**Abstract-** Surface treatments of engineering materials are important for serviceable engineering components. One of the thermo-chemical surface treatments of steel based materials is the boriding process. In this study, low alloy steel substrates were borided by pack boriding process at 900 °C. Experimental indentation tests were conducted on Dynamic Ultra-micro Hardness test machine, under applied peak loads of 800 mN, 1000 mN, 1200 mN and 1400 mN. To get the mechanical properties of FeB layers, the resulting load-unload test data of the samples obtained from the experimental indentation tests were analyzed and curve-fitted in Kick's and Meyer's law for the loading and the unloading part of the load-unload curve respectively. Then, a set of analytical functions that take the pile-up and sink-in effects into account during instrumented sharp indentation were solved using numerical methods. These analytical functions were defined within an identified representative plastic strain,  $\epsilon_p$ , for the Vickers indenter geometry as a strain level that allows for the description of the indentation loading response independent of strain hardening exponent,  $n$ . The mechanical characterization of samples, finite element modeling was applied to simulate the mechanical response of FeB layer on low alloy steel substrate by using ABAQUS software package program.

**Key Words-** Boride Layer, Low alloy steel substrate, Indentation, Yield curve, FEM

### 1. INTRODUCTION

The boriding process is an important thermochemical treatment aimed to improve corrosion resistance and produce surface hardening on ferrous and non-ferrous alloys [1]. In this process, boron atoms diffuse through the surface of a sample creating borides with the base material. Boriding can be made from mixtures of powders, salts, molten oxides, as well as gas mediums and pastes [2]. In solids, paste boriding is an alternative method of sample treatment. It minimizes manual work as compared to powder boriding. It can be used with high work volumes and selective treatments [1–3].

Boriding can be carried out in solid, liquid or gaseous media [4]. Among the various boriding processes, solid-state pack boriding is the most frequently used. And industrial boriding is predominantly applied to steel and ferrous alloys. The pack-boriding process has relatively high processing temperature (800– 1000 C) and long process duration (3–16 h) to obtain an effective boride layer thickness [5, 6]. The powder-pack boriding has the advantages of simplicity and cost-effectiveness in comparison with other boriding processes. In this technique, the boriding agent in powder form is placed into a heat resistant box and samples are embedded into this powder under inert gas atmosphere. At the end of boriding time, the box is cooled at room temperature and then, dust over the samples is removed [7]. The pack usually contains a source of boron, usually boron carbide ( $B_4C$ ) or amorphous boron, an activator to deposit atomic boron at the workpiece and a diluent. Pack boriding involves placing the component in the powder mix and sealing it in a container. The container is then heated up to the required temperature for the required time and cooled in air. Generally, the formation of a monophase ( $Fe_2B$ ) with saw tooth morphology is more desirable than a double phase layer with  $FeB$  and  $Fe_2B$  for industrial applications. A single  $Fe_2B$  layer produces superior wear resistance and mechanical properties [8].

Mechanical properties of bulk materials are usually determined with the help of classical bending or tensile tests; most of the time samples with specific forms are required. It is not sometimes possible to produce such a specific sample in order to evaluate its mechanical properties. Indeed, some materials are brittle, rare or expensive such that the machining of samples is often delicate or inconceivable. Indentation tests are then considered to be suitable tools to evaluate mechanical properties of materials difficult to shape. Depending on the indenter geometry and the load used, indentations are about a few nanometres in depth and a few micrometers wide. Indentation tests are thus a local probe but they can be used for small size samples [9].

### 2.1. Theoretical background of Indentation

The mechanical characterization of materials has long been represented by their hardness values [10]. The work of Tabor is one of the best examples in this area. However, owing to modern computers and advanced numerical methods the understanding of the mechanics in ball indentation [11-13], cone indentation [14] and Vickers Indentation [15] has increased rapidly in recent years. Nanoindenters provide accurate measurements of the continuous variation of indentation load  $P$  down to  $\mu N$ , as a function of the indentation depth  $h$  down to nm. Experimental investigations of indentation have been conducted on many material systems to extract hardness and other mechanical properties and/or residual stresses [16-19].

Figure 1 shows the typical  $P-h$  response of an elasto- plastic material to sharp indentation. During loading, the response generally follows the relation described by Kick's Law:

$$P=Ch^2 \quad (1)$$

where  $C$  is the loading curvature. The average contact pressure,  $p_{ave} = P_{max}/A_{max}$  can be identified with the hardness of the indented material.

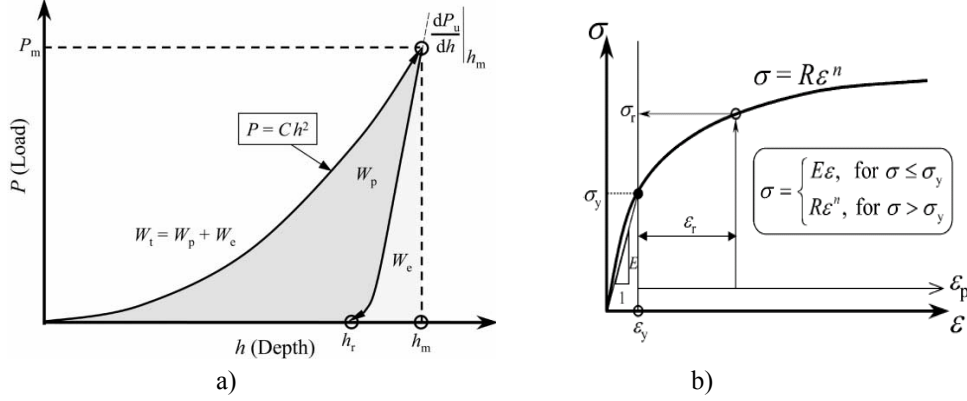


Figure 1. a) Schematic illustration of a typical  $P-h$  response of an elasto-plastic material to instrumented sharp indentation, b) The power law elasto-plastic stress-strain behavior used in the current study

The maximum indentation depth  $h_m$  occurs at  $P_m$ , and the initial unloading slope is defined as  $dP_u/dh$ , where  $P_u$  is the unloading force. The  $W_t$  term is the total work done by load  $P$  during loading,  $W_e$  is the released (elastic) work during unloading, and the stored (plastic) work  $W_p = W_t - W_e$ . The residual indentation depth after complete unloading is  $h_r$ . Plastic behavior of many pure and alloyed engineering metals can be closely approximated by a power law description, as shown schematically in Figure 1.b). A simple elasto-plastic, true stress-true strain behavior is assumed to be:

$$\sigma = \begin{cases} E\varepsilon, & \text{for } \sigma \leq \sigma_y \\ R\varepsilon^n, & \text{for } \sigma \geq \sigma_y \end{cases} \quad (2)$$

where  $E$  is the Young's modulus,  $R$  a strength coefficient,  $n$  the strain hardening exponent,  $\sigma_y$  the initial yield stress and  $\varepsilon_y$  the corresponding yield strain, such that:

$$\sigma_y = E\varepsilon_y = R\varepsilon_y^n \quad (3)$$

Here the yield stress  $\sigma_y$  is defined at zero offset strain. The total effective strain,  $\varepsilon$ , consists of two parts,  $\varepsilon_y$  and  $\varepsilon_p$

$$\varepsilon = \varepsilon_y + \varepsilon_p \quad (4)$$

where  $\varepsilon_p$  is the nonlinear part of the total effective strain accumulated beyond  $\varepsilon_y$ . With equations (3) and (4), when  $\sigma > \sigma_y$ , equation (2) becomes:

$$\sigma = \sigma_y \left( 1 + \frac{E}{\sigma_y} \varepsilon_p \right)^n \quad (5)$$

## 2.2. Determination of Young's Modulus by Indentation

Regarding mechanical properties, hardness testing provides useful information on the strength and deformative characteristics of the materials (elastic modulus, elastic recovery, hardness, etc.). Hardness is a mechanical parameter which is strongly related to the structure and composition of solids. Hence, microhardness is not only a mechanical characteristic routinely measured but it has also been developed as an investigation method of structural parameters in recent years. Therefore, hardness experiments have become more and more important to characterize a material [15, 20].

The characteristic ability of a material to resist penetration of an indenter allows evaluation of a parameter that we know hardness. The indentation hardness of materials is measured in several ways by forcing an indenter having specific geometry (ball, cone, and pyramid) into the specimens' surface.

The conventional microhardness value can be determined from the optical measurement of the residual impression left behind upon load release. In recent decades, the development of depth-sensing indentation equipment has allowed the easy and reliable determination of two of the most commonly measured mechanical properties of materials, the hardness and Young's modulus. The depth-sensing (or dynamic) micro indentation method offers great advantages over conventional Vickers microhardness testing in two aspects. Firstly, apart from microhardness (or micro strength), the method can also provide well-defined mechanical parameters such as elastic modulus of the interfacial zone. Secondly, as load and depth of an indentation are continuously monitored, optical observation and measurement of diagonal length of the indent/impression, which can be difficult and subjected to inaccuracy, is no longer required [21].

Two mechanical properties, namely, elastic modulus  $E$  and microhardness  $H$  can be obtained with the load and penetration depth data. A typical load–penetration depth curve is shown in Fig. 1. During indenter loading, test material is subjected to both elastic and plastic deformation. The three key parameters needed to determine the hardness and modulus are the peak load ( $P_{\max}$ ), the contact area ( $A_c$ ) and the initial unloading contact stiffness ( $S$ ). Similar to the conventional microhardness testing, the micro indentation hardness is usually defined as the ratio of the peak indentation load,  $P_{\max}$ , to the projected area of the hardness impression,  $A_c$ , i.e [21].

$$H = \frac{P_{\max}}{A_c} = \frac{P_{\max}}{26.43h_c^2} \quad (A_c = 26.43h_c^2) \quad (6)$$

Different approaches for deducing the contact depth,  $h_c$ , from the resultant load displacement curve have been purposed and perhaps the most widely used one is that of Oliver and Pharr. The Oliver and Pharr data analysis procedure begins by fitting unloading curve to an empirical power-law relation:

$$P = \alpha(h - h_f)^m \quad (7)$$

Where  $P$  is the indentation load,  $h$  is the penetration depth,  $h_f$  is the final unloading depth and  $\alpha$  and  $m$  are empirically determined fitting parameters. Using the initial part of the unloading curve, both stiffness and contact depth are determined by differentiating Eq. (7) at the maximum depth of penetration,  $h = h_{\max}$ . Then, the stiffness of the contact is given by:

$$S = \frac{dP}{dh} = \frac{2}{\sqrt{\pi}} E_r \sqrt{A_c} \quad \frac{1}{E_r} = \frac{1-\nu^2}{E} + \frac{1-\nu_0^2}{E_0} \quad (8)$$

$E_r$  is called reduced modulus or combined modulus,  $S=dP/dh$  is the experimentally measured stiffness of the upper portion of the unloading data, which is the slope of the curve fitted straight line of the initial part of unloading,  $A$  is the projected contact area of the indenter at maximum loading condition,  $E$  and  $\nu$  are Young's modulus and Poisson's ratio for the specimen, and  $E_0$  and  $\nu_0$  are the same parameter for the indenter.

## 2. FINITE ELEMENT MODELING (FEM) OF PROBLEM

In order to improve the calculation accuracy in the continuous FEM simulation of the nanoindentation, an axisymmetric FEM model of the semi-infinite layered half space was built. To fulfill this target it was necessary to replace the Vickers pyramid through an equivalent cone. This replacement increases the calculation accuracy, since it enables the description of a three-dimensional problem through the application of a plane axisymmetric model. The lack of edge regions of the pyramid indenter negligibly affects the penetration procedure, because these regions are limited in comparison to the whole contact indenter-specimen area. The applied Vickers pyramid and the corresponding defined equivalent cone are demonstrated in the upper part of Figure 3 [22].

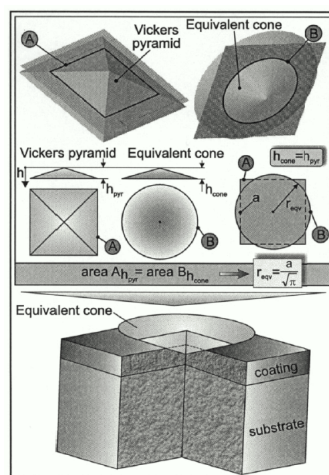


Figure 3. Determination of an equivalent cone to the Vickers pyramid nanoindenter, used in the developed FEM simulation of the nanoindentation



The indenter was meshed by approximately 1500 four-node and 18500 four-node and eight nodes for specimen. Elements were finest and in the central contact area and became coarser outwards and CAX4R and Quad-dominated element types were used. The interaction between the diamond indenter and specimen was modeled by without contact element with no friction.

In this study, we therefore aimed to examine the dynamical hardness measurements and microstructural characterization of boride layers, which were formed on low alloy steels by pack boriding process at 900 °C for 6h process time, in order to determine modulus and hardness values under different applied peak loads and evaluate load dependency of the hardness and modulus of surface layer, FeB. Furthermore, after experimental characterization of hardness and Young's modulus, yield strength, strain hardening exponent of FeB layer is calculated and stress analysis of contact region between FeB and indenter is represented in FEM analysis.

### 3. RESULTS AND DISCUSSION

#### 3.1. Microstructural Investigation

Scanning Electron Microscope (SEM) cross-sectional investigations show that double phase layer from surface to inside of substrate. SEM cross-sectional photograph of low alloy steel, which was borided at 900 °C for 6h, is shown in Figure 5. The structural compositions of layers consist of boron rich phase (FeB) and iron rich phase (Fe<sub>2</sub>B), respectively. FeB formation begins from surface, Fe<sub>2</sub>B phase forms in deeper region because of decreasing boron concentration form surface to inside of substrate. According to the SEM photograph, saw tooth microstructural images show both FeB and Fe<sub>2</sub>B phase.

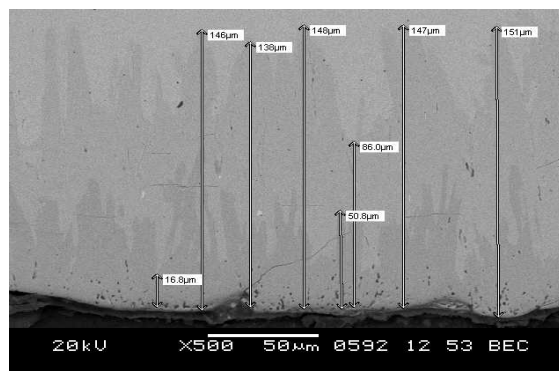


Figure 5. SEM image of borided low alloy steel

#### 3.2 Determination of Mechanical Properties

The load-unload mode (load–displacement) curves shown in Fig. 6 a)-d) represent the 800mN, 1000 mN, 1200mN and 1400mN applied force as a function of

the displacement (elastic and plastic) of the indenter with respect to the initial position of the surface. Three experiments were applied for each force. Table 1 shows Young's modulus, residual depth and maximum depth value of samples under 800mN, 1000 mN, 1200mN and 1400mN applied peak loads.

It is clearly seen from the figures that the extracted reduced elastic modulus also exhibits a strong peak load dependency as shown in Table 1. According to the result, Young's modulus values decrease with increasing applied peak loads.

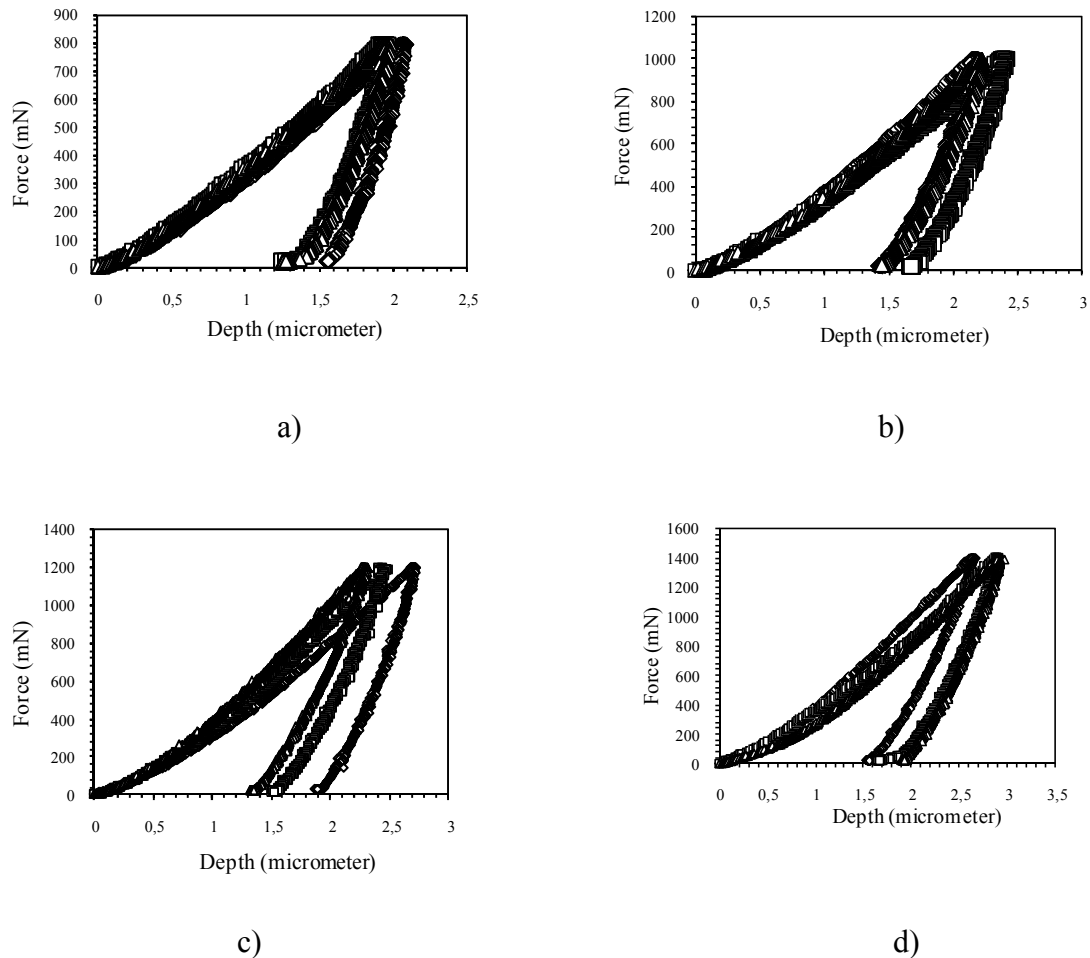
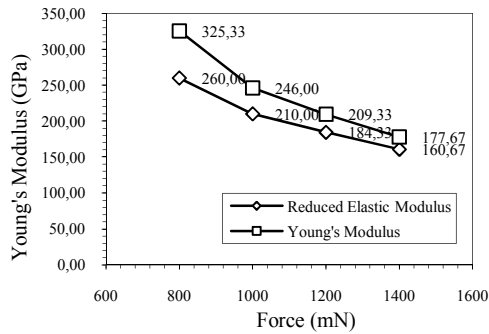


Figure 6. Force –Displacement curves of FeB layer under a) 800 mN, b) 1000 mN, c) 1200 mN and d) 1400 mN

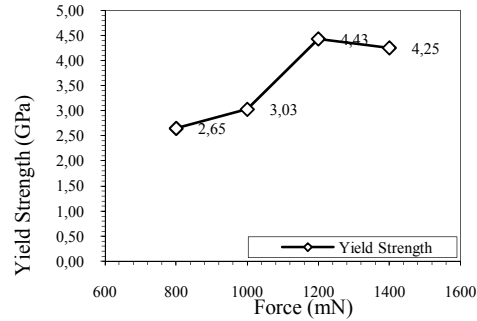
Mechanical properties such as yield strength, and strain hardening exponent of FeB layer were calculated by indentation algorithm as mentioned above. Calculated results were listed in Table 1. According to the Table 2 and Figure 7, indentation load dependency of mechanical properties was seen. Especially, hardness and Young's modulus of FeB layer decrease by increasing applied loads as reduced elastic modulus variations. However, strain hardening exponent of FeB was fixed and did not change by load variations.

Table 1. Indentation and algorithm results of FeB layer under applied loads

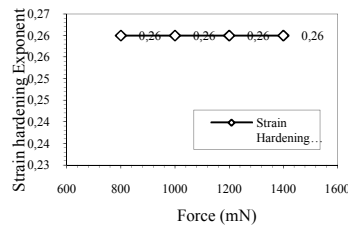
	$P_{max}$ (mN)	$h_{max}$ ( $\mu\text{m}$ )	$h_r$ ( $\mu\text{m}$ )	$h_r/h_{max}$	$E_r$ (GPa)	C (GPa)	E (GPa)	$p_{av}$ (GPa)	$\sigma_y$ (GPa)	n
FeB 800-1	800	2.06	1.56	0.75	291.00	212.31	378.00	15.96	1.97	0.26
FeB 800-2	800	1.95	1.26	0.65	247.00	233.10	303.00	20.48	2.95	0.26
FeB 800-3	800	1.95	1.26	0.65	242.00	233.10	295.00	20.07	3.03	0.26
Avarage	800	1.99	1.36	0.68	260.00	226.17	325.33	18.84	2.65	0.26
FeB 1000-1	1000	2.16	1.44	0.67	200.00	245.81	231.00	15.47	2.94	0.26
FeB 1000-2	1000	2.38	1.67	0.70	212.00	204.03	249.00	14.43	2.68	0.26
FeB 1000-3	1000	2.22	1.44	0.65	218.00	228.84	258.00	17.85	3.37	0.26
Avarage	1000	2.25	1.52	0.67	210.00	226.23	246.00	15.92	3.03	0.26
FeB 1200-1	1200	2.69	1.90	0.70	174.00	187.01	195.00	11.77	2.88	0.26
FeB 1200-2	1200	2.41	1.53	0.63	187.00	224.04	213.00	16.18	4.08	0.26
FeB 1200-3	1200	2.29	1.36	0.59	192.00	261.09	220.00	18.68	6.33	0.26
Avarage	1200	2.46	1.59	0.64	184.33	224.05	209.33	15.54	4.43	0.26
FeB 1400-1	1400	2.64	1.56	0.59	167.00	225.48	186.00	16.32	6.37	0.26
FeB 1400-2	1400	2.88	1.66	0.58	158.00	187.96	174.00	16.08	3.41	0.26
FeB 1400-3	1400	2.91	1.93	0.66	157.00	177.73	173.00	12.33	2.98	0.26
Avarage	1400	2.81	1.72	0.61	160.67	197.06	177.67	14.91	4.25	0.26



a)



b)



c)

Figure 7. a) Young's Modulus b) Yield strength and c) Strain hardening exponent variations of FeB layers with applied peak loads

### 3.3 Finite Element Modeling Results

After calculation of mechanical properties of FeB layer under different indentation force, finite element representation problem was modeled as figure 4. In this study, the FeB layers were modeled as elasto-plastic materials (Young's modulus  $E=325-177$  GPa, Poisson's ratio,  $\nu=0.2$ , yield strength= $2,65-4,25$  GPa, strain hardening exponent,  $n=0.26$ ). Material properties were assumed as above to determine the same penetration depth with experimental results. The substrate was chosen to be commercial steel and was modeled as elastic material with  $E=205$  GPa and  $\nu=0.3$  and yield strength= $280$  MPa, ultimate strength= $600$  and work hardening exponent= $0.2$  [24].

Figure 8 a) and b) show mesh design of the entire model and magnified view of mesh design under Vickers indenter (with  $70.3^\circ$  equivalent angle). Numerical analysis steps include; loading, holding and unloading parts. Figure 10 a) and b) and Figure 11 show loading and unloading step modules with Von Mises stress distribution at contact region of indenter and layer, respectively.

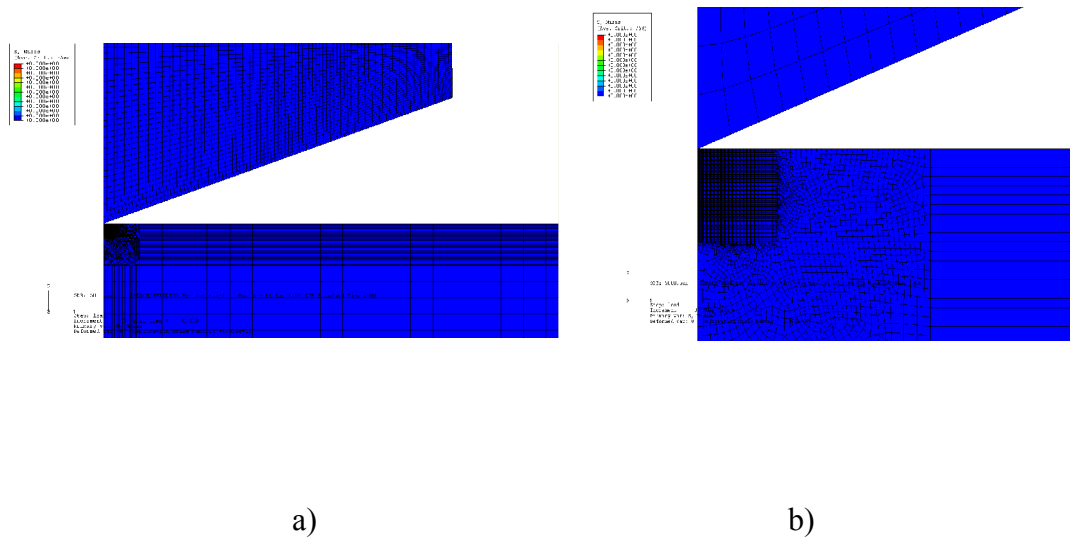


Figure 8. a) Mesh design of in the entire model and, b) Magnified view of mesh design under Vickers indenter

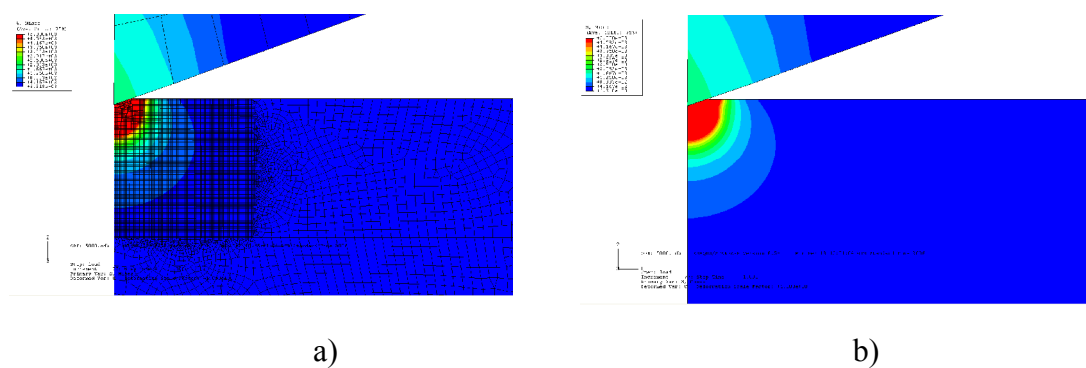


Figure 10. Magnified view of model after loading step under Vickers indenter

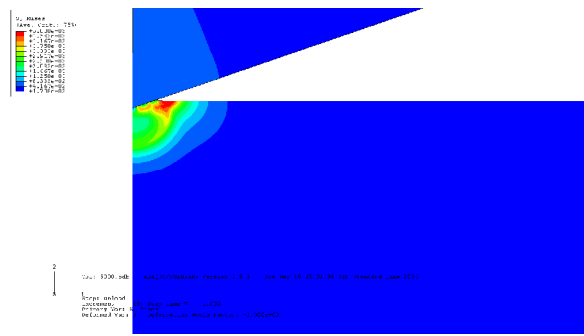


Figure 11. Magnified view of model after unloading step under Vickers indenter

#### 4. REFERENCES

1. A.K. Sinha, Boriding (Boronizing), ASM Handbook, OH, USA. *Journal of Heat Treatment* **4**, 437-447, 1991.
2. A. Graf von Matuschka, *Boronizing, first, Germany*: Carl Hanser, Verlag, 1980.
3. I. Campos, J. Oseguera, U. Figueroa J.A. Garcí'a, O. Bautista and G. Kelemenis, Kinetic study of boron diffusion in the paste-boriding process, *Material Science and Engineering A* **352**, 261–265, 2003.
4. J.A. Davis, P.J. Wilbur, D.L. Williamson, R. Wei and J.J. Vajo, Ion implantation boriding of iron and AISI M2 steel using a high-current density, low energy, broad-beam ion source, *Surface and Coating Technology* **103-104**, 52-57, 1998.
5. K. Bartsch and A. Leonhardt, Formation of iron boride layers on steel by d.c.-plasma boriding and deposition processes, *Surface and Coating Technology* **116-119**, 386-390, 1999.
6. F. Miyashita and K. Yokota, Plasma-assisted low temperature boridation of pure iron and steels, *Surface and Coating Technology* **84**, 334-337, 1996.
7. M. Keddad and S.M. Chentouf, A diffusion model for describing the bilayer growth (FeB/Fe<sub>2</sub>B) during the iron powder-pack boriding, *Journal of Applied Surface Science* **252**, 393-399, 2005.
8. I. Uslu, H. Comert, M. Ipeki, F.G. Celebi, O. Ozdemir and C. Bindal, Evaluation of Borides Formed on AISI P20 Steel, *Material and Design* **28**, 55-61, 2007.
9. B. Guillaume F. Boschini, A. Rulmont, M. Ausloos and R. Cloots, Influence of the shaping effect on hardness homogeneity by Vickers indentation analysis, *Journal of the European Ceramic Society* **26**, 3191-3196, 2006.
10. D. Tabor, *Hardness of Metals*, Charendon Press, Oxford, 1951.
11. R. Hill, F.R.S., B. Storakers and A.B. Zdunek, A theoretical of the Brinell hardness tests. *Proceeding of the Royal Society London A* **423**, 301-330, 1989.
12. E.R. Kral, K. Komvopoulos and D.B. Bogy, Elastic-plastic finite-element analysis of repeated indentation of a half-space by a rigid sphere, *Journal of Applied Mechanics* **60**, 829-841, 1993.
13. A.E. Giannakopoulos, P.-L. Larsson and R. Vestergaard, Analysis of Vickers indentation, *International Journal of Solids and Structure* **31**, 2679-2708, 1994.
14. T.A. Laursen and J.C. Simo, A study of the mechanics microindentation using finite-elements, *Journal of Materials Research* **7**, 618-626, 1992.
15. A.E. Giannakopoulos and S. Suresh, Determination of elastoplastic properties by instrumented sharp indentation, *Scripta Materialia* **40**, 1191-1198, 1999.

16. M.F. Doener and W.D. Nix, A method for determining the data from depth-sensing indentation instruments, *Journal of Materials Research* **1**, 601-609, 1986.
17. G.M. Pharr and R.F. Cook, Instrumentation of a conventional hardness tester for load–displacement measurement during indentation, *Journal of Materials Research* **5**, 847-851, 1990.
18. W.C. Oliver and G.M. Pharr, An improved technique for determining hardness and elastic-modulus using load and displacement sensing indentation experiments, *Journal of Materials Research* **7**, 1564-1583, 1992.
19. A. Bolshakov, W.C. Oliver and G.M. Pharr, Influences of stress on the measurement of mechanical properties using nanoindentation: Part II. Finite element simulations, *Journal of Materials Research* **11**, 760-768, 1997.
20. E. Atar, C. Sarioglu, U. Demirler, E.S. Kayali and H. Cimenoglu, Residual stress estimation of ceramic thin films by X-ray diffraction and indentation techniques, *Scripta Materialia* **48**, 1331-1336, 2003.
21. O. Uzun, U. Kolemen, S. Celebi and N. Guclu, Modulus and hardness evaluation of polycrystalline superconductors by dynamic microindentation technique, *Journal of the European Ceramic Society* **25**, 969-977, 2005.
22. K.-D. Bouzakis, N. Michailidis and G. Erkens, Thin hard coatings stress–strain curve determination through a FEM supported evaluation of nanoindentation test results, *Surface and Coating Technology* **142**, 102-109, 2001.
23. C.A. Brookes, *Properties of diamond*, Academic Press, New York, 1979.
24. J.L. He and S. Veprek, Finite element modeling of indentation into superhard coatings, *Surface and Coating Technology* **163-164**, 374-379, 2003.